



AFRL-OSR-VA-TR-2013-0562

**COMPRESSIVE SAMPLING FOR NON-IMAGING REMOTE
CLASSIFICATION**

DAVID BRADY

DUKE UNIVERSITY

**10/22/2013
Final Report**

DISTRIBUTION A: Distribution approved for public release.

**AIR FORCE RESEARCH LABORATORY
AF OFFICE OF SCIENTIFIC RESEARCH (AFOSR)/RSE
ARLINGTON, VIRGINIA 22203
AIR FORCE MATERIEL COMMAND**

REPORT DOCUMENTATION PAGE			<i>Form Approved</i> <i>OMB No. 0704-0188</i>	
Public reporting burden for this collection of information is estimated to average 1 hour per response, including the time for reviewing instructions, searching existing data sources, gathering and maintaining the data needed, and completing and reviewing this collection of information. Send comments regarding this burden estimate or any other aspect of this collection of information, including suggestions for reducing this burden to Department of Defense, Washington Headquarters Services, Directorate for Information Operations and Reports (0704-0188), 1215 Jefferson Davis Highway, Suite 1204, Arlington, VA 22202-4302. Respondents should be aware that notwithstanding any other provision of law, no person shall be subject to any penalty for failing to comply with a collection of information if it does not display a currently valid OMB control number. PLEASE DO NOT RETURN YOUR FORM TO THE ABOVE ADDRESS.				
1. REPORT DATE (DD-MM-YYYY) 13-09-2013		2. REPORT TYPE Final		3. DATES COVERED (From - To) 15-06-2010 - 14-06-2013
4. TITLE AND SUBTITLE Compressive sampling for non-imaging remote classification			5a. CONTRACT NUMBER	
			5b. GRANT NUMBER FA9550-10-1-0321	
			5c. PROGRAM ELEMENT NUMBER	
6. AUTHOR(S) Brady, David J. Marks, Daniel L. Mrozack, Alex Tsai, Tsung-Han			5d. PROJECT NUMBER	
			5e. TASK NUMBER	
			5f. WORK UNIT NUMBER	
7. PERFORMING ORGANIZATION NAME(S) AND ADDRESS(ES) Duke University Office of Research Administration 2200 W. Main Street Suite 710 Durham, NC 27705-4677			8. PERFORMING ORGANIZATION REPORT NUMBER	
9. SPONSORING / MONITORING AGENCY NAME(S) AND ADDRESS(ES) AFOSR Dr. Kent Miller 875 N. Randolph St. Room 3112 Arlington VA 22203-1768			10. SPONSOR/MONITOR'S ACRONYM(S) AFOSR	
			11. SPONSOR/MONITOR'S REPORT NUMBER(S)	
12. DISTRIBUTION / AVAILABILITY STATEMENT Distribution is unlimited				
13. SUPPLEMENTARY NOTES				
14. ABSTRACT Compressive sampling strategies using image-space modulation for polarization and spectral data cube reconstruction and interferometric subsampling for coherence measurement were demonstrated. Compressive millimeter wave imaging systems were demonstrated using the common mathematical and physical analysis framework. A new design for multiscale wide aperture high resolution telescopes was developed. The new approach may combine image plane compression with parallel multiscale cameras to enable wide area object capture at the physical limits of spatial, spectral and temporal resolution.				
15. SUBJECT TERMS compressive imaging, spectral imaging, polarization imaging, terahertz imaging				
16. SECURITY CLASSIFICATION OF:			17. LIMITATION OF ABSTRACT	18. NUMBER OF PAGES 23
a. REPORT Unclassified	b. ABSTRACT Unclassified	c. THIS PAGE Unclassified		
				19b. TELEPHONE NUMBER (include area code) 919-660-5394

Table of Contents

Objectives	2
Results	2
Sensor platforms and telescropy	3
Image-space coding	3
Spectral Imaging	4
Space-time Imaging	7
Polarization Imaging	8
Coherence coding	14
Terahertz imaging.....	17
Personnel supported	20
Publications	20
Inventions	20
References	21

Objectives

Historically, imaging systems have struggled to match human perception. Imagers have been built with red-green-blue sensors to match human color space, with 1-10 megapixel focal planes to match human acuity and with 30 millihertz temporal resolution to match human sensitivity. Of course, microscopes and telescopes have been used for centuries to extend the resolution of human vision. In practice, however, these instruments simply magnify conventional 30 frame per second, three color megapixel images to match human scale.

Recently, however, system designers have begun to focus on cameras that vastly exceed the spectral, temporal and spatial resolution of human vision. Such cameras, limited by diffraction and photon statistics rather than human perception, might capture 10^{15} or more spatio-spectral-temporal pixels per second¹. The primary challenge in capturing such a large data volume will be to communicate, process and utilize the information it contains. Current cameras use up to 1W per resolved megapixel, suggesting that a petapixel camera might require a gigawatt of power.

Physical layer compression is the solution to this power challenge. By sensing only pixels of interest and by multiplexing these pixels into compressed signal volumes, the power required per pixel can be reduced by many orders of magnitude. This AFOSR program focused on demonstrating compressive imaging systems in which traditional focal strategies are abandoned in favor of physical layer coding. Since the goal of these systems is information transfer maximization, rather than focal image formation, we referred to these designs as “non-imaging.” We were particularly interested in the demonstration of object analysis from compressively coded measurements².

Results

“Compressive sampling for non-imaging classification” yielded many innovations in the applications of compressive sampling to remote sensing. These included a broadband ultraviolet to near-infrared wavelength compressive spatio-spectral imager, two designs for a snapshot spectro-polarization imager, a compressive coherence imager to resolve objects through turbulence, novel temporal compressive sampling enabling rapid motions and high frame rate video to be determined from low-bandwidth encoded video, and a new architecture for wide-field, high resolution telescopes for sky surveys. The program was also supplemented with support from the United States Army to allow the compressive sampling methodology to be applied to tomographic terahertz imaging.

The multiscale wide field telescope design is a platform for integrating spatio-spectral-temporal coding strategies for very high pixel count wide field imaging. While we did not complete construction of the multiscale telescope, it is useful to begin this report with a summary of the telescope design as a motivating factor for integration of the computational imaging systems. Following this summary we review our results with three different coding strategies and field models. Compressive spectral, polarization and temporal imaging was achieved via *image space modulation*, which uses a coded aperture in an intermediate image plane. Terahertz and coherence imaging, in contrast uses direct interferometric detection of fields or coherence functions. Our results with interferometric systems are reviewed following the image space discussion.

Sensor platforms and telescoping

Ordinary telescopes require optics of increasing complexity to achieve both wide fields and high resolution. Multiscale design has already been used in the DARPA AWARE program for wide-field cameras^{3,4}. Remote sensing may also benefit from this technology using these multiscale telescopes⁵. The designs include both reflecting and refractive types spanning 300 megapixels to 40 gigapixels, and up to 60 degrees field-of-view with 1 arcsec IFOV at the seeing limit of the atmosphere. An example below is a proposed reflective design that can be made relatively inexpensive compared to the separate telescopes it replaces. It is the equivalent of 88 8-inch telescopes created by placing a microcamera array in front of a spherical mirror of 760 mm diameter.

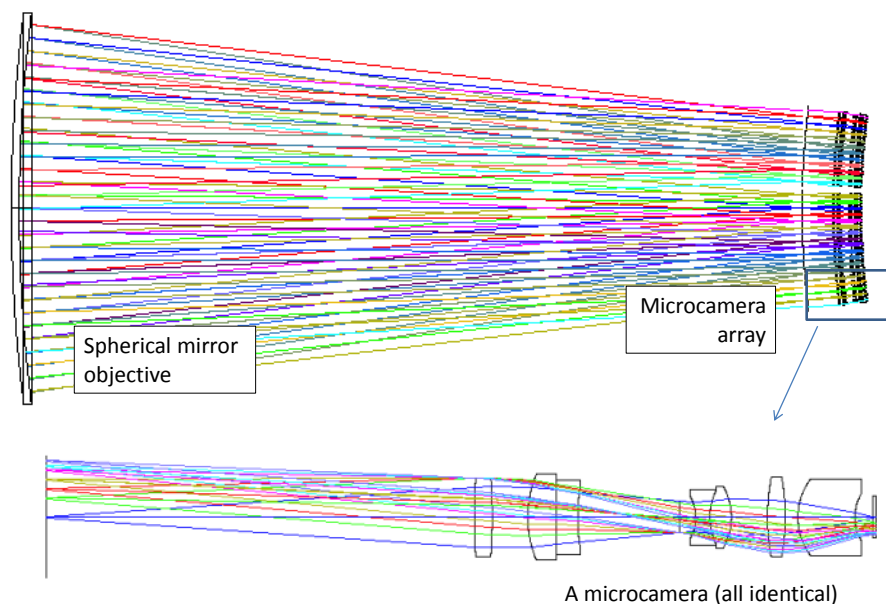


Fig.1 A reflective telescope design with a microcamera array in front a spherical mirror. Each microcamera consists of seven inexpensively fabricated spherical glass elements.

We believe that future space situational awareness networks will greatly benefit from multiscale telescope designs, especially those with spectral and polarization based encoding incorporated into them for classification and identification. The innovations of the program can all contribute to the overall goals originally set out for the program.

Image-space coding

The most effective compressive coding strategy for focal imaging consists of modulation in intermediate image planes. This approach allows

Spectral Imaging

To achieve a goal of the project to infer wide spectral content from a small number of sampled frames, we constructed a ultraviolet-visible-near infrared coded aperture snapshot spectral imager (CASSI) with 300 to 800 nm wavelength sensitivity. The design achieved significantly higher spatial and spectral resolution than earlier instruments. It is based on a symmetric Cooke triplet design with an unusual optical design strategy: a BK7 element is used as a “flint” element to balance the calcium fluoride crown elements. This way, an extremely wide bandwidth was achromatized. Fig 2. is a diagram of this optical instrument.

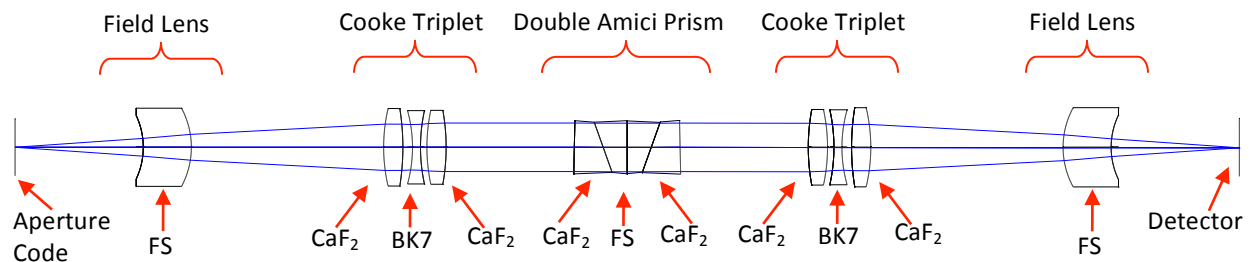


Fig. 2 The relay lens for UV-CASSI, which focuses the aperture code onto the monochrome detector. The multiconfiguration setting in Zemax was used to optimize lens parameters considering post tolerance performance. This reduced tolerance requirements and fabrication costs.

The constructed instrument is shown below in Fig. 3, with a silicon UV sensitive detector on the left, and a UV wideband objective on the right. The coding mask is placed directly into the field of the objective lens with the mask actuated by a piezo element. The piezo element allows the position of the mask to shift to encode multiple code features into a given position on the image.

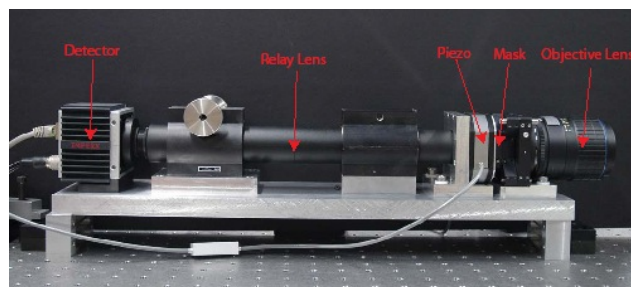


Fig. 3. The UV-CASSI instrument, including objective lens, coded aperture, relay lens/dispersive element, and detector.

A sparse reconstruction method based on total variation minimization was used to infer the spatio-spectral data cube from 24 code mask shifts. An Ox-Eye daisy as shown in Fig. 4, with ultraviolet features otherwise invisible to humans (but visible to bees) was used to test the ability of the system to capture the visible and ultraviolet spectral data together and then distinguish it using the compressive inference technique.

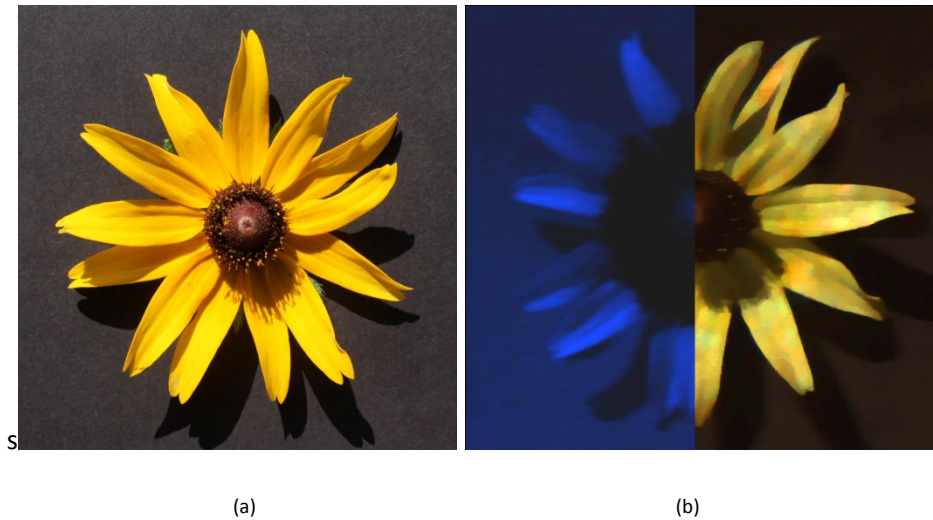


Fig.4 (a) RGB image of flower in sunlight, (b) CASSI image of flower in sunlight, with UV on the left and visible on the right.

The 24 decoded spectral channels of the daisy are shown in Fig 5. The ultraviolet features of the daisy are clearly seen, as well as green, yellow, and red reflectivity, but blue is absent. The absence of infrared features is also notable. A simulated reconstruction using the HYDICE reference spectral image is shown in Fig. 6 with 4 and 32 frame reconstructions. The compressive approach allows one to trade image fidelity for speed flexibility as needed ⁶.

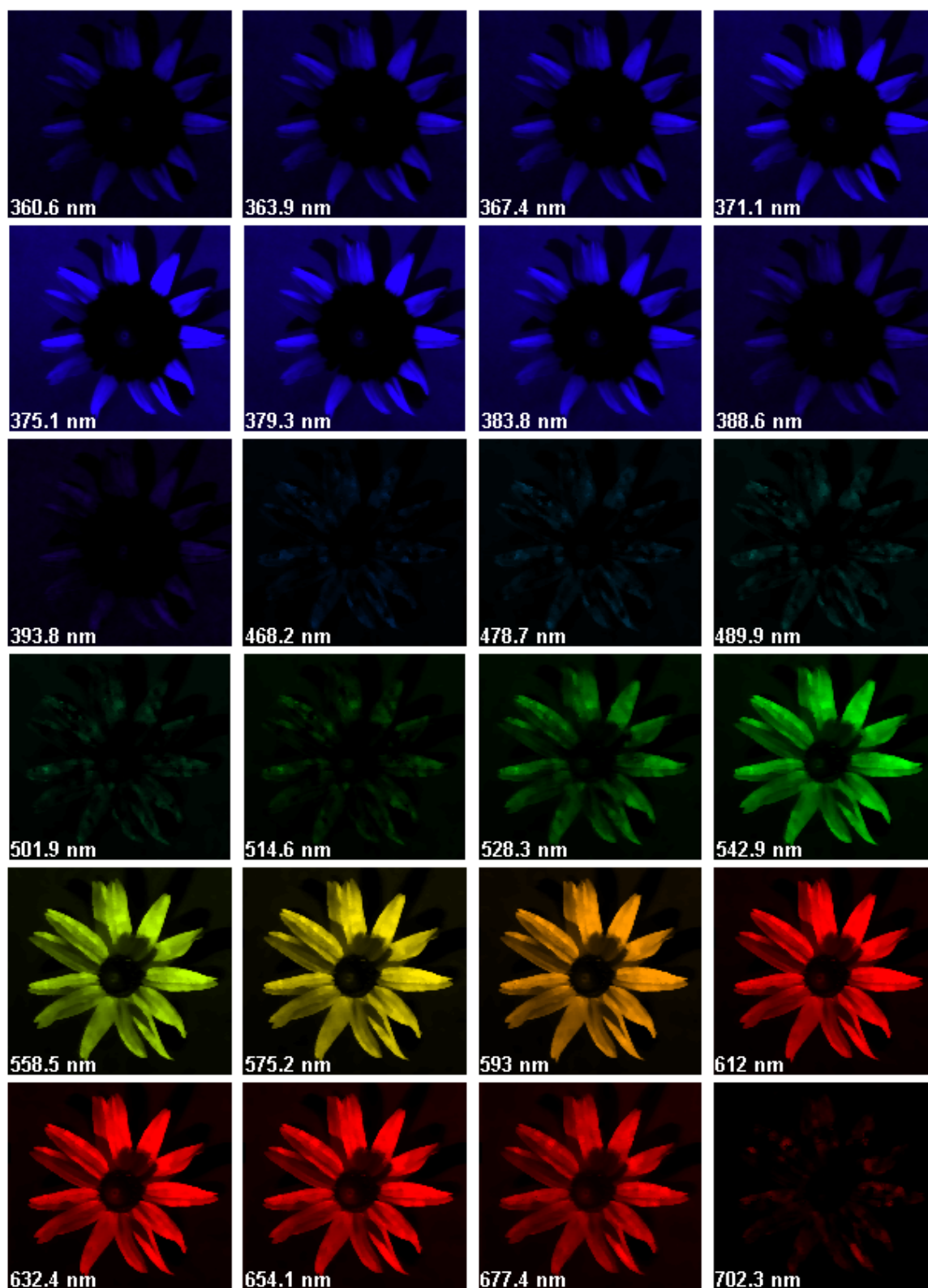


Fig. 5 UV-Visible reconstruction from 360nm to 700nm, taken using multiple frames in direct sunlight.

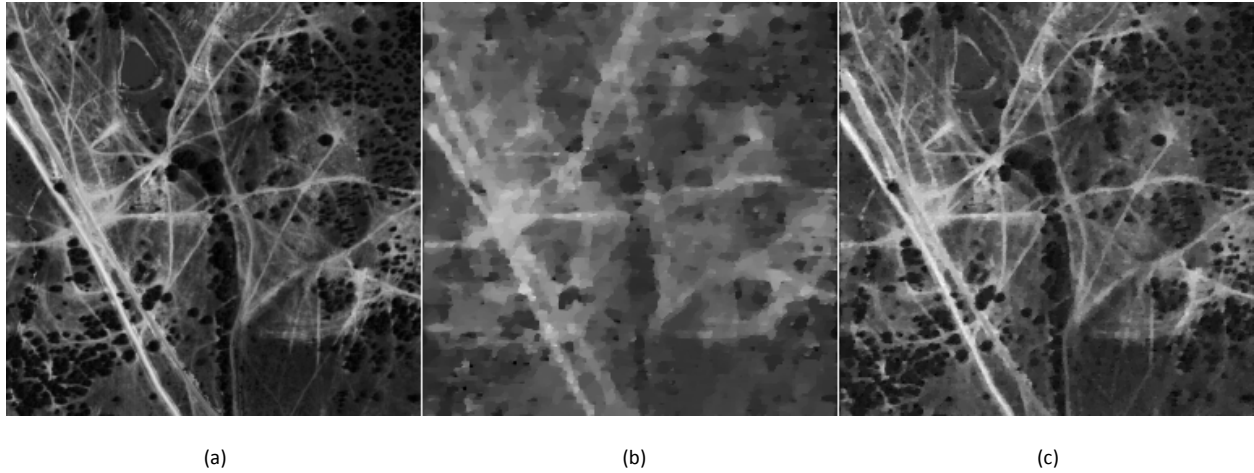


Fig. 6 Left: cropped, 595nm channel of the HYDICE data set; middle: 4-Snapshot reconstruction; Right: 32-frame reconstruction.

Space-time Imaging

Another application of compressive sensing based on the spectral imaging approach allows for temporal encoding onto spatial structure. This allows relatively slow sensors to be used for high frame rates. This work, which we believe has great applications in tracking of rapidly moving targets, is a direct spinoff of the spectral work. As an object moves, so does the coding mask, and their relative motions encode a unique spatial code onto the image which is used to infer the motion.

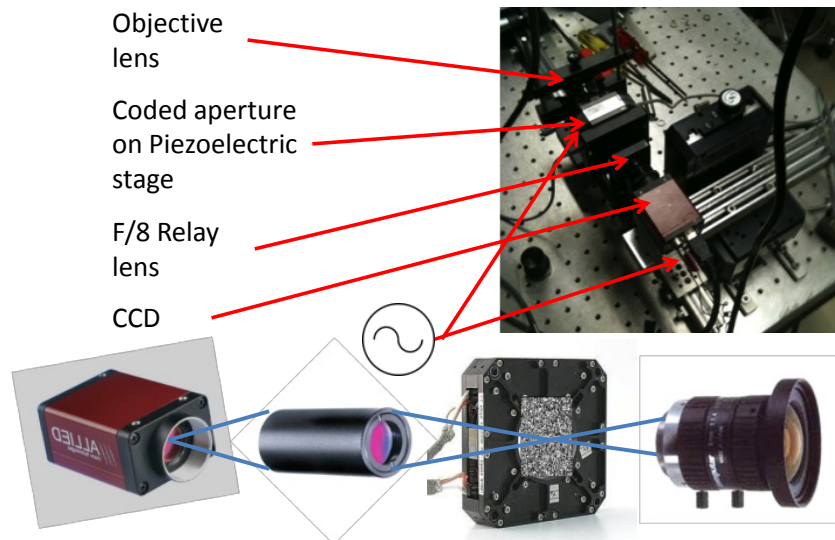


Fig. 7 Compressive temporal imager. A mask, similar to that used in compressive aperture snapshot spectral imaging, is moved during an exposure to encode the temporal events during the exposure onto the image spatial structure.

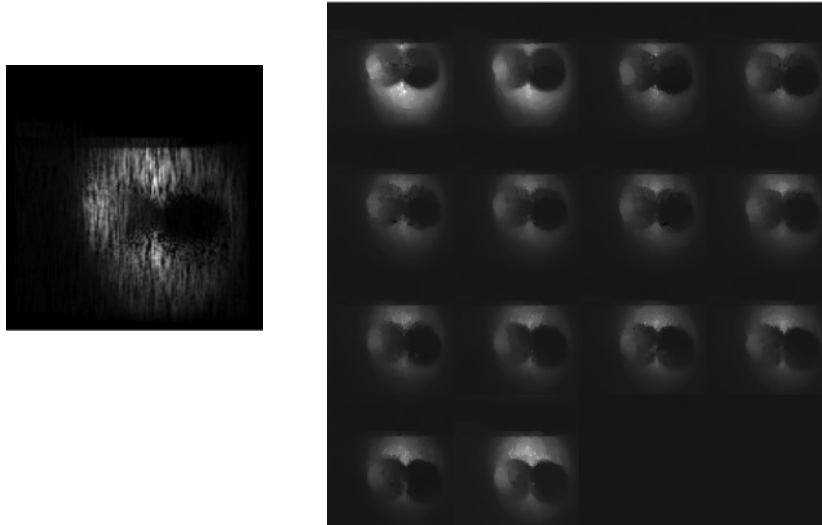


Fig. 8 Compressive inference of fast temporal motion. From the single captured frame on the left, the entire video sequence of 14 frames was decoded.

We recently have demonstrated a temporal compression of 14:1 as shown in Fig. 8⁷. A single frame was taken over which the mask was moved by 14 code block lengths. This encoded the motion of a falling ball (and its shadow) into various code patterns as seen by the “grain” in the encoded image. By decoding this grain, the video sequence of 14 frames was found, showing the motion of the ball. We believe much greater temporal compression is possible, with 30:1 or even 100:1 being possible. Such a technology may be very useful to encode fast motions onto slow sensors such as microbolometer infrared sensors .

Polarization Imaging

Spectral polarization imaging is another application which based on spatially encodes the higher dimensional information⁸. This allows the spectral and polarization state insensitive detector to capture the color and polarized images. We believe this work can be applied in the area of remote sensing and surface analysis. To achieve this goal, we constructed a coded aperture snapshot spectral polarization imager (CASSPI) with the sensitivity of 400 to 680 nm in wavelength and two Stokes parameters.

A schematic layout of CASSPI is shown in Fig. 9. An objective lens images the scene on the coded aperture plane. The coded aperture provides the spatial modulated pattern to encode the scene over all

wavelengths in the object cube. Relay optics project the encoded cube from this plane to the detector array through birefringent crystals, which shear the object cube to its wavelength and polarization-dependent location. Finally, the detector array records the intensity pattern, which includes the spatial, spectral and polarization modulated information of the object.

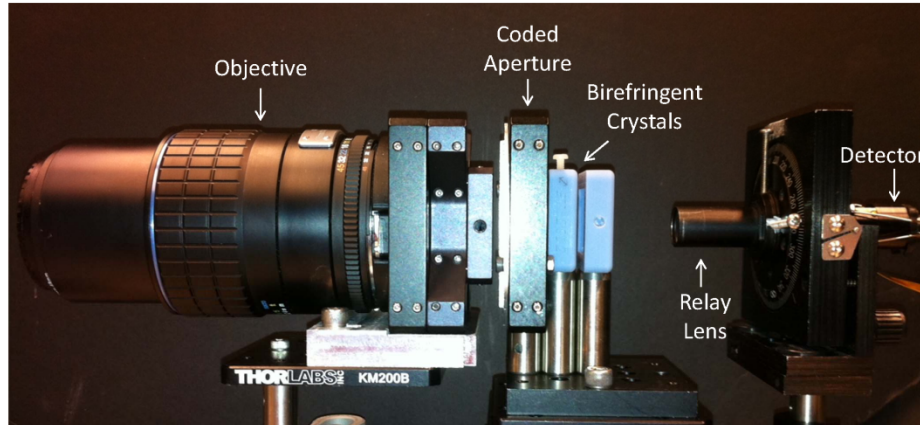


Fig. 9. The experimental prototype of the CASSPI system, including objective lens, coded aperture, birefringent crystals, relay lens, and detector.

The birefringent crystals provide polarization and spectral dispersion. Fig. 10 illustrates the design of the birefringent crystals and their dispersion relationship. Both crystals are made of calcite, due to its strong birefringent and high transmission within the visible wavelength. The optical axes of the first and the second calcite plates have been chosen as 45° relative to the y - z plane and x - z plane. Therefore, the parallel polarized light of the first crystal will become the orthogonally polarized light for the second crystal. For example, considering an un-polarized incident light propagating through this crystal pair. The extraordinary ray (e ray) will be shifted along the $-x$ direction by the first crystal and then pass through the second crystal as the ordinary ray (o ray) without any deviation. The o ray, which is outgoing from the first crystal, becomes the e ray and then it will be dispersed by the second crystal along the $-y$ direction. This image-displacing effect splits images into two orthogonal polarization states. The displaced images are also spectrally dispersed due to materials dispersion.

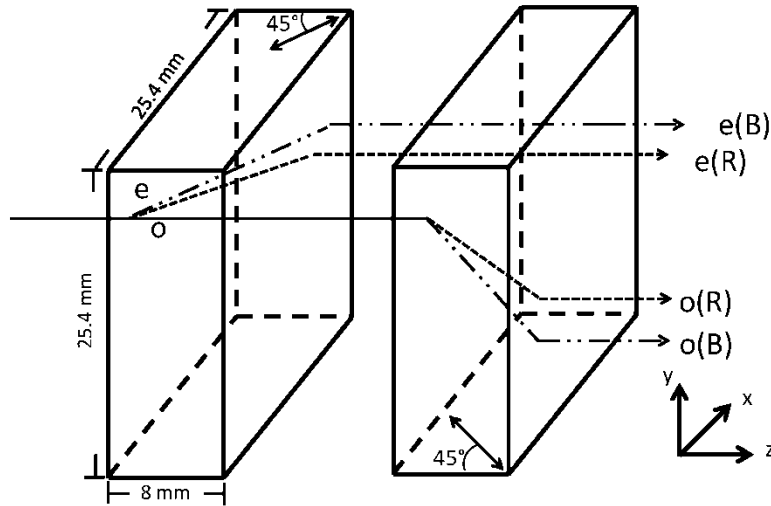


Fig. 10. The design of the birefringence crystal.

A total variation optimization based reconstruction was used to retrieve the spatio-spectral and polarization data cube from a snapshot measurement. We used a negative 1951 USAF resolution test chart, which was back illuminated by a tungsten light bulb and filtered by a linear polarizer, to test the camera.

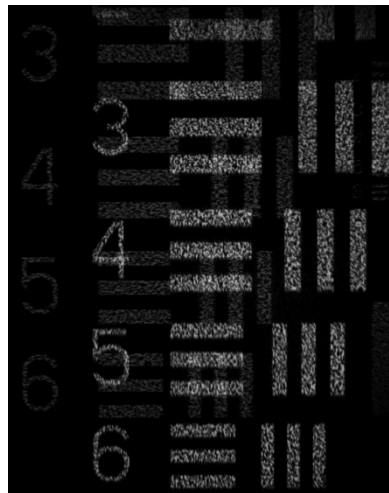


Fig. 11. Measured data of the scene including a negative 1951 USAF resolution test chart. Given the splitting and dispersion by the birefringent crystal, this measurement consists of spectral-spatial and polarization-spatial overlap of the coded modulated image of the test chart.

Fig. 11 shows the detector measurement of the test chart. As shown in the figure, the measurement on the detector plane is the superposition of two groups of overlapping images; each image is modulated by the coded pattern. The overlapping in the measurement was due to the dispersion and splitting that redistributed the intensity of the incident image by the two birefringent crystals.

Figures 12 and 13 present the reconstruction of 19 wavelength channels and two Stokes parameters between 400 and 680 nm. Since the azimuth angle of the polarizer was located at 30°, the ideal ratio between S1 (polarization difference) and S0 (irradiance) is 0.5.

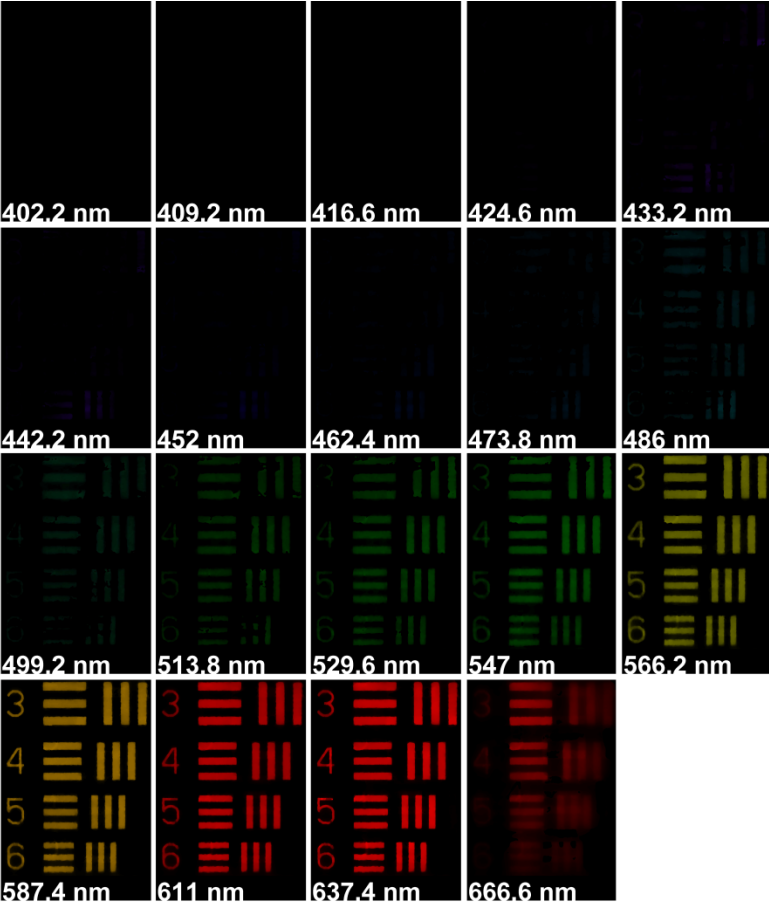


Fig. 12. Spectral and polarization reconstruction in 19 wavelength channels between 400 and 680 nm in irradiance terms.

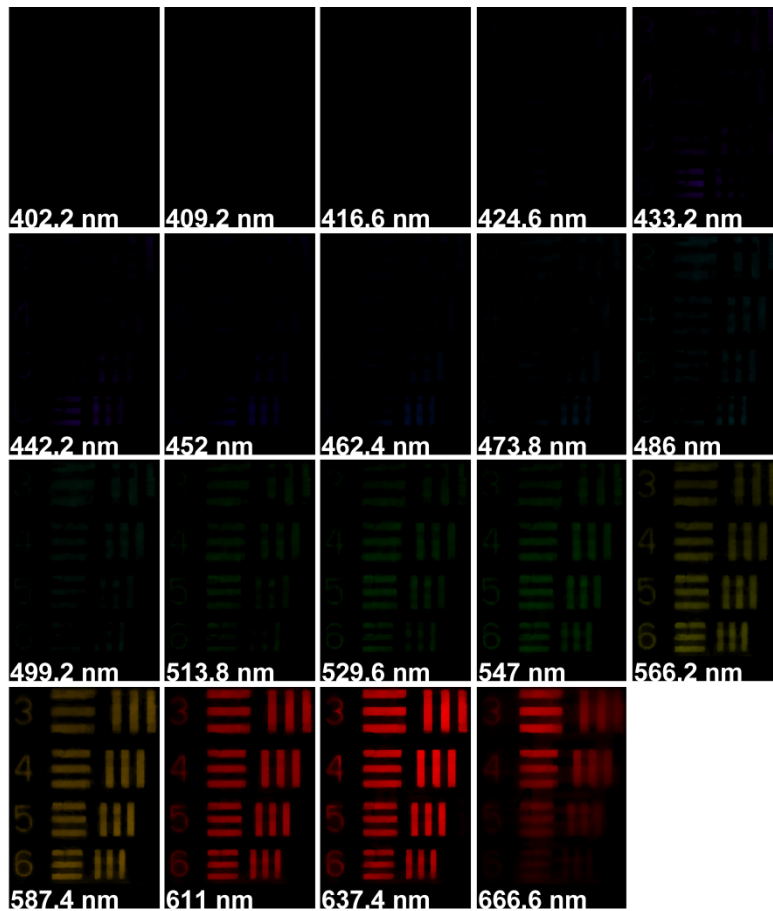


Fig. 13. Spectral and polarization reconstruction in 19 wavelength channels between 400 and 680 nm in polarization difference terms.

Another approach to achieve the spectral polarization imaging is to use a liquid crystal on silicon (LCoS) spatial light modulator (SLM) to jointly code spatial, spectral and polarization information without using any dispersive element. We demonstrate compressive sampling of megapixel multidimensional image on a two-dimensional (2D) detector array. The 4D data cube includes megapixels in spatial domain, three wavelength channels and their horizontal and vertical polarized irradiance.

The system layout of the camera is shown in Fig. 14. A series of lenses projects the scene on the SLM, which is the intermediate image plane. A random voltage pattern is applied on the SLM, which provides a spectral and polarization dependent amplitude modulation to encode the object when its image pass through the wave-plate and the polarizer. The modulated image will then recorded by the color detector.

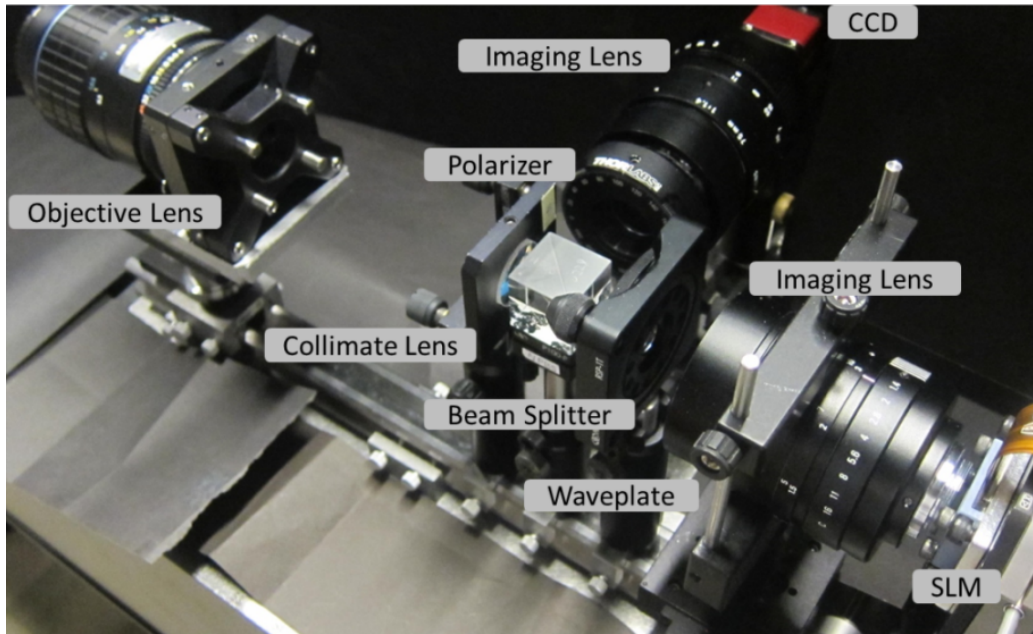


Fig. 14. System layout of the SLM based spectral polarization camera, including an objective lens, a collimate lens, a beam splitter, a achromatic quarter wave-plate, two imaging lens, a LCoS based SLM, a polarizer, and a color CCD.

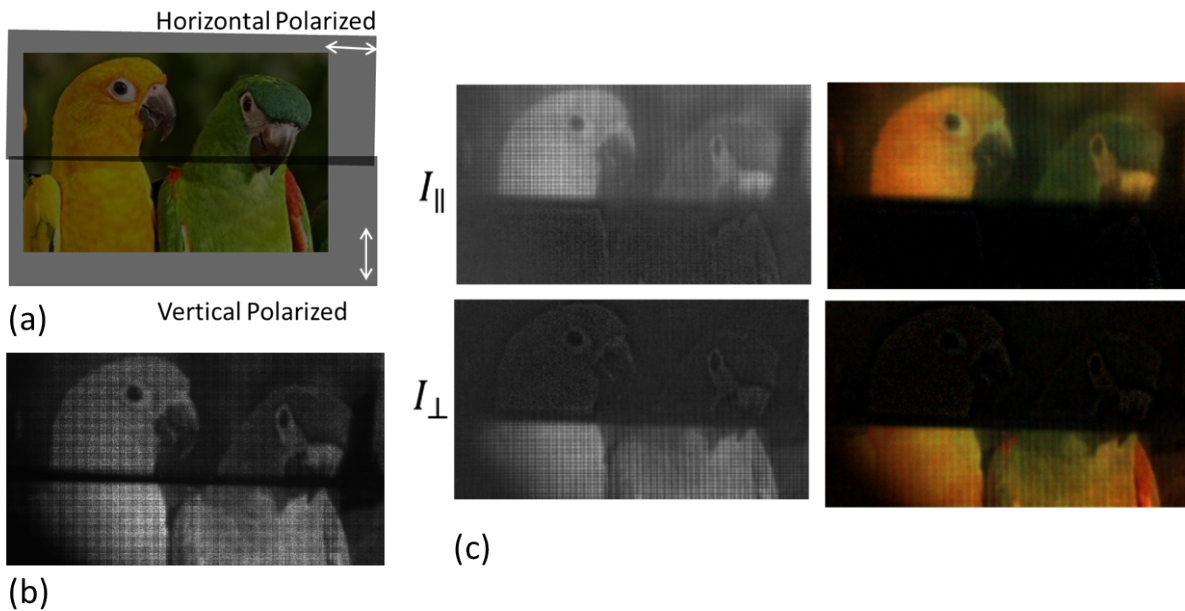


Fig. 15. Experimental result of this spatial light modulator based snapshot spectral polarization imaging. (a)The test object was filtered by two sheet polarizer with different orientation in azimuth angle. (b) The raw measurement data comes from the detector. (c)The reconstruction result (left) of two polarization channels and their corresponding color images after demosaic the color filter.

Fig. 15 shows an example of using a spectral polarization imaging. A color printed picture combined with two polarization filter in was used in the system validation. The raw image from the detector array was used in the reconstruction process. The reconstruction was using the sparsity in the frequency domain instead of the spatial domain by projecting the measurement by discrete cosine transform. The reconstruction successfully separates the horizontal and the vertical polarized information from the measurement. After demosaic the color filter pattern, three channels spectral information can also be retrieved by this snapshot 2D irradiance measurement. This work was presented at the 2013 Frontiers in Optics conference.

Coherence coding

Another application of compressive sensing is the measurement of objects through turbulence using compressive coherence sensing⁹. The coherence of an incoherently radiating object that is corrupted by turbulence contains both the object structure and a random turbulence phase. However, this phase is common to all objects being imaged. We demonstrated that by using compressive inference, we could measure the mutual intensity of a turbulence-corrupted source using a rotational shearing interferometer, infer the turbulence, and produce a well-resolved image.

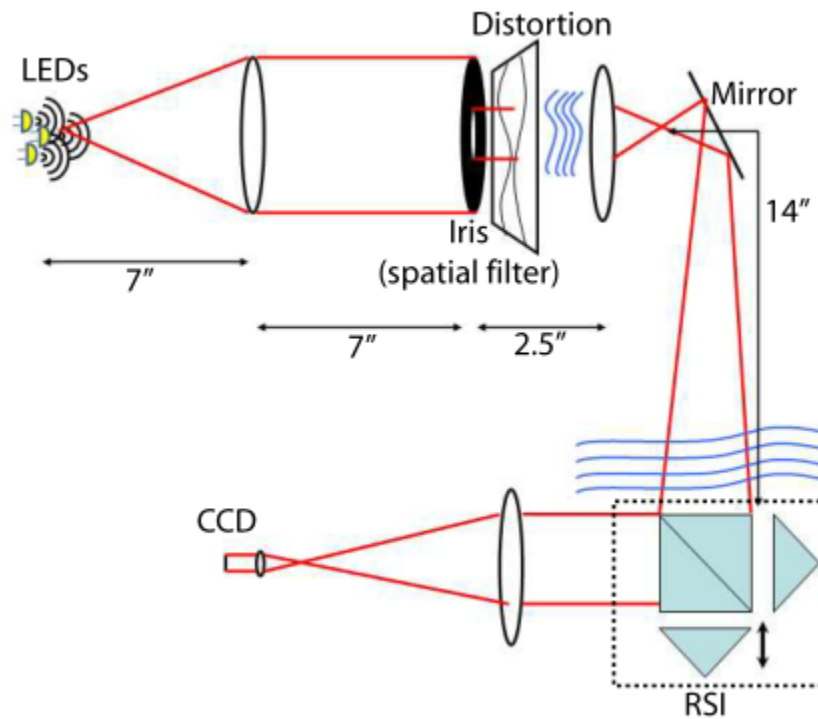
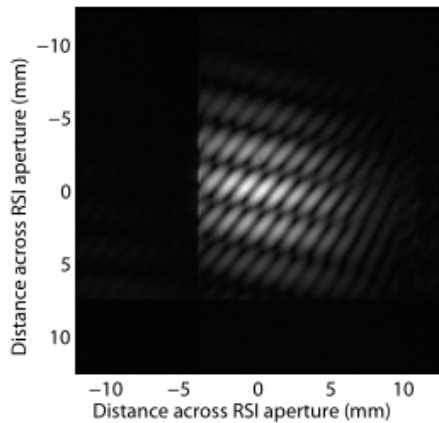


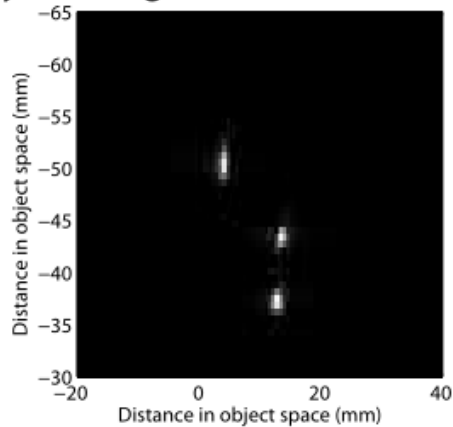
Fig. 16 A rotational shearing interferometer used for measuring coherence. Three light emitting diodes are collimated to place their image at infinity. A distorting plate simulating turbulence is placed in the path of the field. This field is then sheared to two different rotations and combined to form an incoherent hologram on a CCD sensor.

The rotational shearing interferometer of Fig. 16 is used to measure samples of the mutual intensity of the turbulence-corrupted source. A piece of silicone cured into a wavy pattern using a heat gun served as a simulated turbulence source. In the absence of turbulence the two-dimensional Fourier transform of the mutual intensity is the desired object intensity pattern. However, a corrupting turbulence phase causes a change in the point spread function of the system. A sparsity constraint was used to find the turbulence phase that minimized the blurring and therefore sharpened the intensity pattern. Two situations were compared: without and with turbulence. Fig 17 shows the reconstruction of the three LEDs in the source, which have been correctly inferred to have little or no phase turbulence corruption.

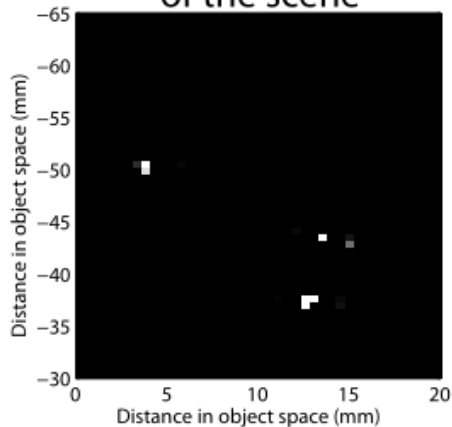
(a) Measured 2D subset of samples of the mutual intensity



(b) Image of the scene using the VCZ theorem



(c) Estimate of the image of the scene



(d) Estimate of OPD due to turbulence

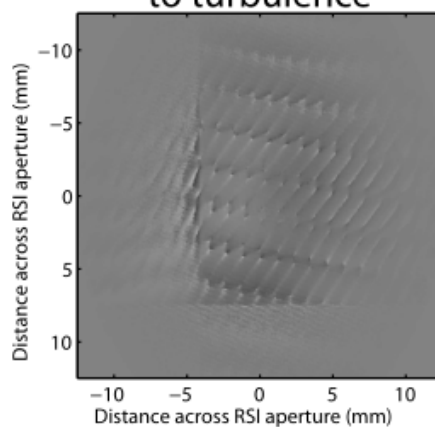


Fig. 17 Reconstruction of a three LED object without turbulence. The van Cittert-Zernike theorem, which assumes no turbulence is present, produce a high-quality image. This image is not significantly altered because the OPD is correctly estimated to have no turbulence phase.

Figure 18 is an example including the silicone phase turbulence plate. Using the standard Van Cittert-Zernike theorem imaging, the three LEDs are unresolvable. However, the algorithm can use the sparsity constraint to find the corrupting turbulence phase and correct the mutual intensity to what it would have been if no turbulence is present, thereby allowing the Van Cittert-Zernike theorem to be used to reconstruct the object.

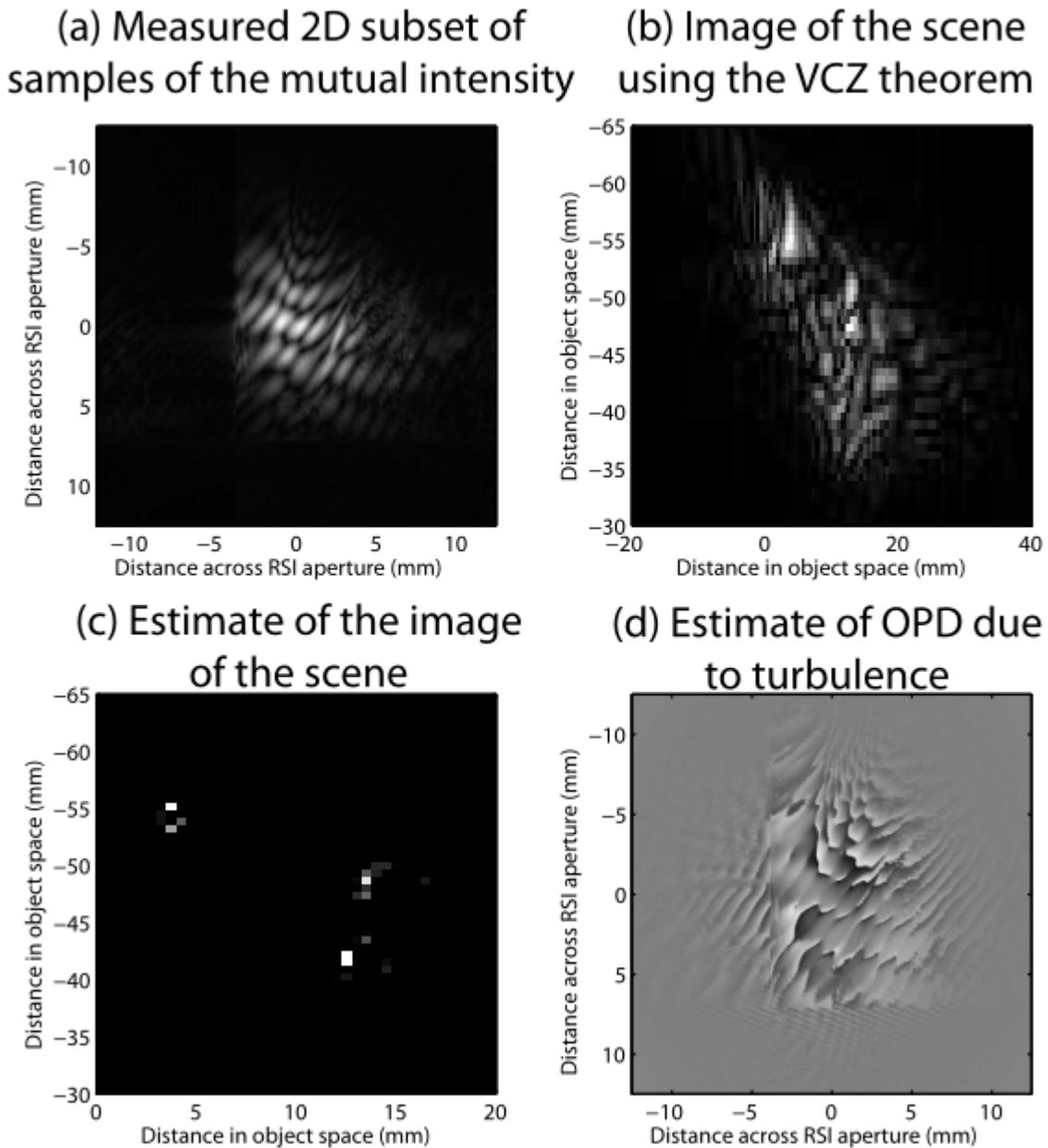


Fig.18 Reconstruction of a three LED object with turbulence. The three LEDs are indistinguishable using the van Cittert-Zernike theorem due to the turbulence that is present. The turbulence phase can be inferred using a sparsity constraint, enabling the undistorted mutual intensity function to be inferred to produce the corrected image.

Terahertz imaging

This program supported research into synthetic aperture imaging for THz systems¹⁰. In the THz region of the spectrum detectors are expensive, however generation of coherent radiation is not difficult. This leads to the ability to image by a procedure similar to synthetic aperture radar (SAR) and interferometric synthetic aperture microscopy (ISAM). Synthetic aperture imaging uses a frequency and 1d or 2d lateral sweep to generate range cross-range 2d images or range cross-range cross-range 3d images. These methods are beneficial to Army operations, as they can be used to detect sparse metal in porous materials. This is beneficial for observing the explosive force of a new weapon. The first demonstration of this capability was published in “Terahertz interferometric synthetic aperture tomography for confocal imaging systems” in Optics Letters. Fig. 19 shows the setup of the experiment. Fig. 20 shows the results from the experiment. Both figures are from the aforementioned publication.

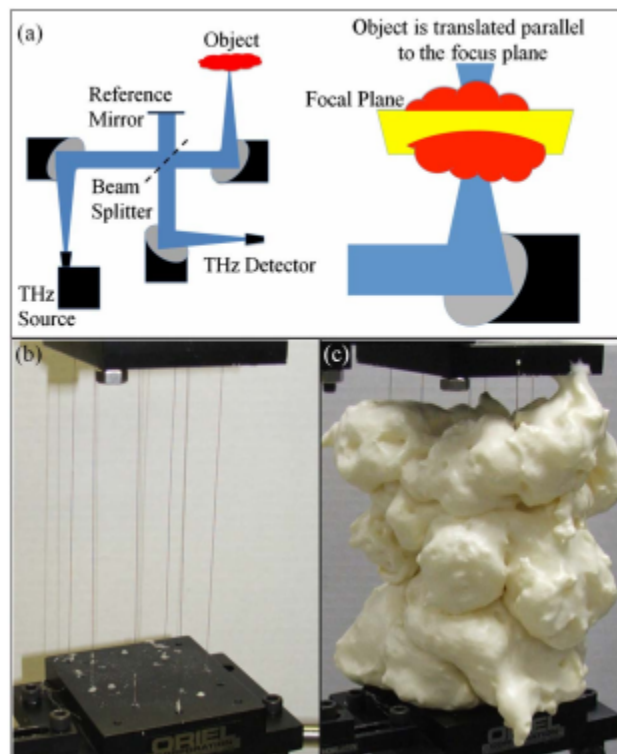


Fig. 19 The experimental setup for a synthetic aperture imager at a center frequency of 355GHz. The wires were imaged both with and without being embedded in the foam.

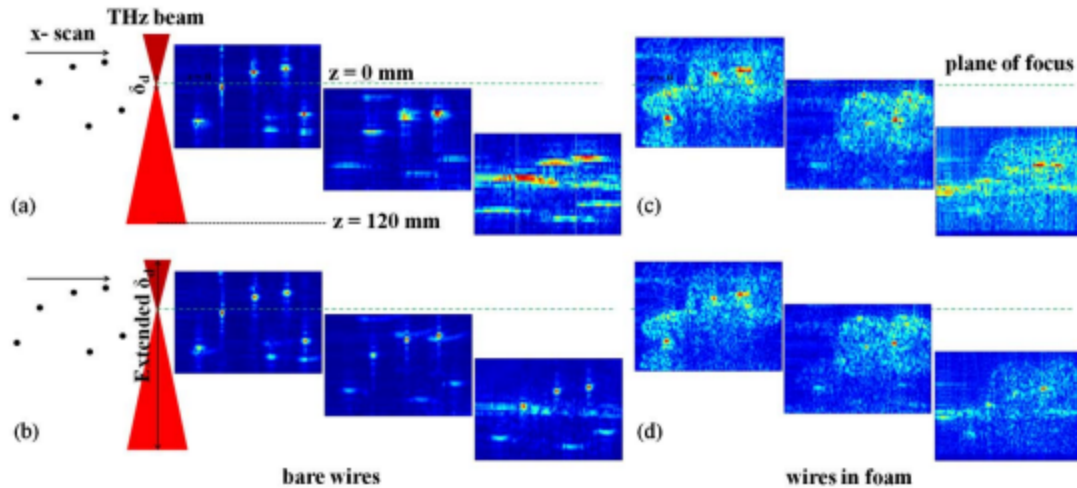


Fig. 20 Imaging results for the setup in Fig. 12. The points are moved to different depths to show depth invariant resolution of the ISAM reconstruction technique.

While the full scan results are useful demonstrations of the feasibility of imaging through porous materials at these frequencies, the time it takes to complete a full scan is large. The largest contributor to the scan time is the acceleration and deceleration times, because maintaining an accurate location for the stage is important if the data is to be processed coherently. For this reason, we would like to generate images in as few lateral measurements as possible. The classic way to do this is through simple compressed sensing with l_1 minimization to regularize the solution. To show feasibility for this, we took one of the datasets from the above experiment and downsampled in the lateral sampling direction. The resulting image from %30 of the lateral samples matches that of the fully sampled image nearly identically. This is an encouraging result, as it would speed up the acquisition time drastically. A comparison of the downsampled and fully sampled reconstructions is shown in Fig. 21. This work was presented at the 2012 Imaging and Applied Optics Conference under the title “Coherent Terahertz Holographic and Tomographic Imaging.”

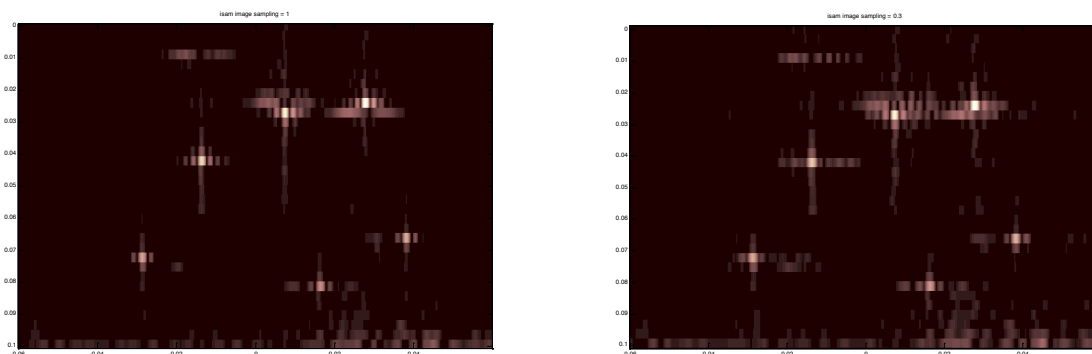


Fig. 21 The left image shows the compressive reconstruction of the object in Fig. 12 with full sampling, while the right image shows the reconstruction with %30 of the lateral sampling.

While compressive sampling is an effective strategy, it is hard to determine an optimal sampling scheme for any given object in the class. That is why random sampling patterns are often chosen. To be even more aggressive in our approach we would like to adjust our sampling scheme on the fly. This comes from the philosophically similar, but mathematically different approach of adaptive sensing. The approach that we performed our first experiment with requires a small and specified number of scatterers. Fig. 22 shows a typical adaptive sensing path for a detecting the location of a single point scatterer. Fig. 23 shows the ability of the algorithm to estimate the lateral location of the point scatterer vs. lateral measurement. This also shows speedups of close to %30 on average, but does so in a way such that if more measurements are necessary that ability is built in automatically.

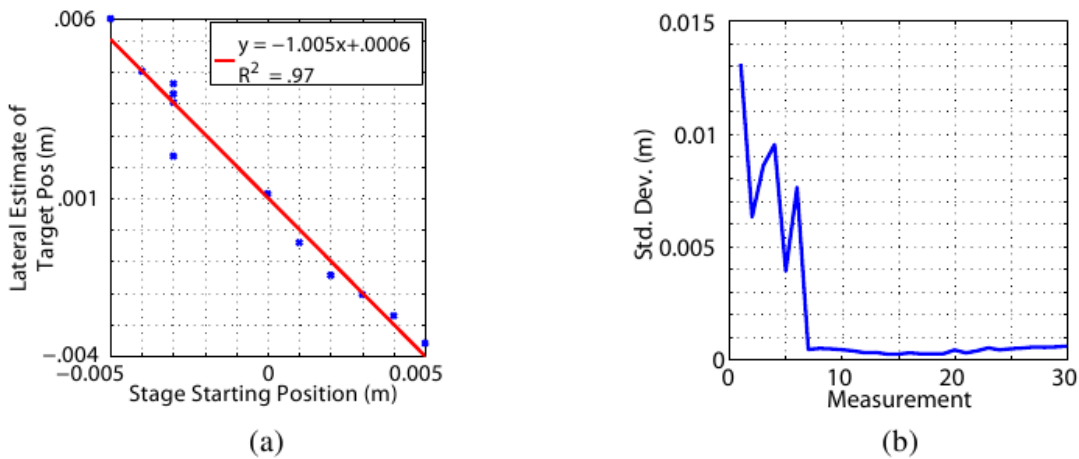


Fig. 22 The regression line for what the lateral estimate of the point is for different locations on the stage (the stage coordinate system is reversed relative to the estimation coordinate system) is left, while the convergence to that regression line is shown right. The estimation converges after 7 or 8 lateral measurements on average, while a full measurement set for that resolution and field of view would be 20 lateral measurements.

The standard deviation from the regression line converges to an error of approximately .5mm. This is an example of super-resolution since the beam waist is roughly 3mm at the NA and frequencies used for this experiment ($\sim 100\text{GHz}$ and $\sim .25\text{NA}$). This work was presented at the 2013 Frontiers in Optics conference under the title “Adaptive Scanning for Synthetic Aperture Imagers”

The next step in the adaptive scanning for THz project will be to use Bayesian compressed sensing to combine the adaptive and compressive paradigms. This will allow for relaxation of the requirement that we specify the number of scatterers exactly to perform adaptive sampling.

This has been joint work with AMRDEC members Henry Everitt and Martin Heimbeck.

Personnel supported

David Brady, Professor of Electrical and Computer Engineering, was the principal investigator for this project.

Daniel Marks, Research Associate Professor of Electrical and Computer Engineering, worked on terahertz imaging and coding strategies.

Kerkil Choi, Postdoctoral Fellow, worked on decompressive inference algorithms.

Orges Furxhi, Postdoctoral Fellow, worked on compressive millimeter wave imaging.

Kalyani Krishnamurthy, Postdoctoral Fellow, worked on compressive inference algorithms.

David Kittle, graduate research assistant, worked on spectral imaging for non-imaging object analysis.

Tong Wu, graduate research assistant, worked on imaging system analysis.

Tsung-Han Tsai, graduate research assistant, developed compressive spectro-polarization cameras.

Alex Mrozack, graduate research assistant, developed decompressive interferometric imaging systems and analyzed non-imaging coding strategies.

Publications

1. Kittle, D., K. Choi, A. Wagadarikar, and D.J. Brady, *Multiframe image estimation for coded aperture snapshot spectral imagers*. *Applied Optics*, 2010. **49**(36): p. 6824-6833.
2. Wagadarikar, A.A., D.L. Marks, K. Choi, R. Horisaki, and D.J. Brady, *Imaging through turbulence using compressive coherence sensing*. *Optics Letters*, 2010. **35**(6): p. 838-840.
3. Zhang, Q., R. Plemmons, D. Kittle, D. Brady, and S. Prasad, *Joint segmentation and reconstruction of hyperspectral data with compressed measurements*. *Applied Optics*, 2011. **50**(22): p. 4417-4435.
4. Heimbeck, M.S., D.L. Marks, D. Brady, and H.O. Everitt, *Terahertz interferometric synthetic aperture tomography for confocal imaging systems*. *Optics Letters*, 2012. **37**(8): p. 1316-1318.
5. Mrozack, A., D.L. Marks, and D.J. Brady, *Coded aperture spectroscopy with denoising through sparsity*. *Optics Express*, 2012. **20**(3): p. 2297-2309.
6. Marks, D.L. and D.J. Brady, *Wide-field astronomical multiscale cameras*. *Astronomical Journal*, 2013. **145**(5).
7. Tsai, T.H. and D.J. Brady, *Coded aperture snapshot spectral polarization imaging*. *Applied Optics*, 2013. **52**(10): p. 2153-2161.

Inventions

1. Multiscale gigapixel telescopes, Duke Invention Disclosure 4043

References

- 1 Brady, D. J. *et al.* in *Computational Imaging XI Vol. 8657 Proceedings of SPIE* (eds C. A. Bouman, I. Pollak, & P. J. Wolfe) (2013).
- 2 Zhang, Q., Plemmons, R., Kittle, D., Brady, D. & Prasad, S. Joint segmentation and reconstruction of hyperspectral data with compressed measurements. *Applied Optics* **50**, 4417-4435 (2011).
- 3 Brady, D. J. *et al.* Multiscale gigapixel photography. *Nature* **486**, 386-389, doi:10.1038/nature11150 (2012).
- 4 Brady, D. J. & Hagen, N. Multiscale lens design. *Optics Express* **17**, 10659-10674 (2009).
- 5 Marks, D. L. & Brady, D. J. WIDE-FIELD ASTRONOMICAL MULTISCALE CAMERAS. *Astronomical Journal* **145**, doi:10.1088/0004-6256/145/5/128 (2013).
- 6 Kittle, D., Choi, K., Wagadarikar, A. & Brady, D. J. Multiframe image estimation for coded aperture snapshot spectral imagers. *Applied Optics* **49**, 6824-6833, doi:10.1364/ao.49.006824 (2010).
- 7 Llull, P. *et al.* Coded aperture compressive temporal imaging. *Optics Express* **21**, 10526-10545, doi:10.1364/oe.21.010526 (2013).
- 8 Tsai, T. H. & Brady, D. J. Coded aperture snapshot spectral polarization imaging. *Applied Optics* **52**, 2153-2161 (2013).
- 9 Wagadarikar, A. A., Marks, D. L., Choi, K., Horisaki, R. & Brady, D. J. Imaging through turbulence using compressive coherence sensing. *Optics Letters* **35**, 838-840 (2010).
- 10 Heimbeck, M. S., Marks, D. L., Brady, D. & Everitt, H. O. Terahertz interferometric synthetic aperture tomography for confocal imaging systems. *Optics Letters* **37**, 1316-1318 (2012).